AIAA JOURNAL
Vol. 40, No. 6, June 2002

Characterization of a Silicon-Micromachined Thermal Shear-Stress Sensor

Mark Sheplak,* Venkataraman Chandrasekaran,† Anthony Cain,‡
Toshikazu Nishida,§ and Louis N. Cattafesta III¶
University of Florida, Gainesville, Florida 32611-6250

A detailed characterization is presented of a silicon-micromachined thermal shear-stress sensor employing a thin-film platinum-sensing element on top of a silicon-nitride membrane that is stretched over a vacuum cavity. The sensor was operated in a constant current mode and characterized using a four-point probe configuration to isolate the sensor response from the effects of external compensation circuitry. The characterization results consist of static sensitivity data at multiple overheat ratios (maximum of 11 mV/Pa at an overheat of 1.0), pressure sensitivity spectra (<1 μV/Pa), noise floor spectra (100 nV/$\sqrt{\text{Hz}}$), and direct dynamic calibration data (up to 7 kHz). Noise floor measurements reveal a minimum detectable shear stress of 9 μPa/Hz, thus resulting in a sensor dynamic range of over 100 dB (9 μPa–1.7 Pa).

Introduction

ACCURATE, time-resolved measurements of wall shear stress are critical for a physical understanding of complex flow phenomena.[1] At moderate Reynolds numbers, typical length scales of interest are on the order of 100 μm or less, and the typical timescales require a usable bandwidth of 10 kHz to capture the spectrum of turbulent fluctuations.[2] Such stringent requirements point toward micromachined sensors as a potential solution.

Much like their macroscopic counterparts,[1] existing micromachined shear-stress sensors can be grouped into two distinct classes: direct techniques, such as floating-element devices,[3–11] or indirect techniques, such as hot wires or hot films.[5,12–21] Löfdahl and Gad-el-Hak presented a review of microelectromechanical systems (MEMS) sensors for turbulent flows that included shear-stress sensors.[22] Naughton and Sheplak also reviewed existing MEMS shear-stress sensors and discussed the advantages and disadvantages of using these devices to obtain quantitative shear-stress data.[23]

In this paper, we present a detailed characterization of a silicon-micromachined thermal shear-stress sensor. The sensor employs a thin-film platinum-sensing element on a silicon-nitride membrane stretched over a vacuum cavity. The next section contains a review of the key operational characteristics of the sensors, including low-frequency substrate conduction effects. Subsequent sections present the experimental setup and results for static sensitivity data at multiple overheat ratios, pressure sensitivity, noise floor spectra, and direct, in situ dynamic calibration data. The paper is concluded with a discussion of the results and suggestions for future work.

Background

The operating principle of an indirect, thermal technique is simply the transduction of temperature to voltage.[24] During operation, the sensing element is resistively heated to a temperature greater than the gas temperature defined by the nondimensional thermal overheat ratio

$$\alpha_T = (T_s - T_g)/T_g = \Delta T/T_g \tag{1}$$

where T_s and T_g are the absolute sensor and gas temperatures, respectively. As the temperature of the sensor varies with changes in the flow environment, so does its resistance and, hence, the joulean heating rate. The convection of heat from the sensor is related to the wall shear stress by a theoretical or empirical correlation and is measured by monitoring changes in the temperature-dependent resistance of the sensing element:

$$R_s = R_r[1 + \alpha(T_s - T_r)] \tag{2}$$

where R_s is the sensor resistance at T_s, R_r is the sensor reference resistance at an absolute reference temperature T_r, and α is the thermal coefficient of resistance (TCR).

The thermal inertia of the sensor ultimately limits its dynamic range, and an external compensation circuit is typically used to extend the measurement bandwidth. The fluid dynamics community has long used various compensation schemes to measure time-resolved skin friction.[24,25] Constant current (CC) and constant voltage (CV) modes use CC and CV, respectively, to provide heating power to the sensor. These modes do not regulate sensor temperature, and thus, the sensor resistance varies with changes in the fluid temperature and shear stress. Consequently, when thermal overheat ratio is specified for CC and CV, it corresponds to zero mean flow and the nominal fluid temperature. In comparison, the constant temperature mode provides heating power to the sensor via a feedback to maintain a constant sensor temperature and, thus, resistance.[26] In any case, the design of an appropriate dynamic compensation technique requires a thorough understanding of the uncompensated sensor dynamics.

Because thermal shear-stress sensors are temperature-resistive transducers that respond to heat transfer rate, a theoretical or empirical correlation is needed to relate the measured Joulean heating rate to the wall shear stress.[1] Classical hot-film theory states that the relationship between the wall shear stress and heat transferred to the fluid is given by[27]

$$Nu \equiv qL/k_f \Delta T = 0.807(PrL^{+2})^{\frac{1}{3}} = 0.807Pe^{\frac{1}{3}} \propto \tau^{\frac{1}{3}} \tag{3}$$

where Nu is the Nusselt number, Pr is the Prandtl number $c_p\mu/k_f$, Pe is the Peclet number PrL^{+2}, k_f is the thermal conductivity of the

Presented as Paper 2001-0247 at the AIAA 39th Aerospace Sciences Meeting, Reno, NV, 8–11 January 2001; received 16 April 2001; revision received 8 November 2001; accepted for publication 21 November 2001.

*Assistant Professor, Department of Aerospace Engineering, Mechanics and Engineering Science, Interdisciplinary Microsystems Group. Member AIAA.

†Graduate Student, Department of Aerospace Engineering, Mechanics and Engineering Science, Interdisciplinary Microsystems Group. Student Member AIAA.

‡Graduate Student, Department of Electrical and Computer Engineering; currently Microsystems Project Engineer, U.S. Air Force Research Laboratory, AFRL/MLPO, Wright–Patterson Air Force Base, Dayton, OH 45433-7707.

§Associate Professor, Department of Electrical and Computer Engineering, Interdisciplinary Microsystems Group.

¶Assistant Professor, Department of Aerospace Engineering, Mechanics and Engineering Science, Interdisciplinary Microsystems Group. Senior Member AIAA.

fluid, c_p is the specific heat of the fluid, μ is the dynamic viscosity, q is the heat flow per unit area, L^+ is L normalized by the viscous length scale $L^+ = u_\tau L/\upsilon$, u_τ is the friction velocity $\sqrt{(\tau/\rho)}$, ρ is the fluid density, and $\nu = \mu/\rho$ is the kinematic viscosity. The assumptions for the analysis yielding this result are that the thermal boundary thickness at the trailing edge of the heated film, δ_T, is entirely contained within a linear velocity profile, the boundary-layer assumption holds ($\delta_T \ll L$), and there is no conduction to the substrate.

Haratonidis discusses the validity of these assumptions in Ref. 1. By comparing the models of Ling[28] and Ackerberg et al.,[29] he showed that, for $Pe < 100$, the boundary-layer approximation is not valid, the heat transfer to the flow does not scale with $\tau^{1/3}$, and the sensor becomes less sensitive with decreasing Peclet number. The uniqueness of the correlation between heat transfer and wall shear stress for laminar and turbulent boundary layers requires that the thermal boundary be contained in the viscous sublayer, $\delta_T < 5y^+$. Using Ling's solution for the thermal boundary-layer thickness,[28] this constraint becomes $L^+ < 4.1Pr$. The fine spatial resolution and thermal isolation of micromachined thermal sensors usually results in a low Peclet number flow when used in air, and thus the classical one-third-power law scaling is not expected to be valid at moderate shear stress levels.[30] When these scaling relations are evaluated, the effects of substrate conduction must be accounted for because the effective length L_e of the sensor can be much larger than L due to substrate heating.[1]

The dynamic response of thermal sensors is further complicated by the frequency-dependent heat conduction into the supporting structure, for example, the substrate for hot films[24,25,31] and prongs for hot wires.[32] This unsteady heat conduction creates a low-frequency rolloff in the gain factor of the frequency-response function, as well as a corresponding frequency-dependent phase lag. If not compensated for, the frequency-dependent phase and gain factors will produce errors in spectral and correlation data. In addition, the unequal dynamic and static sensitivities preclude the use of stochastic calibration techniques.[33] The difficulties associated with the modeling of a time-dependent conjugate heat transfer problem inhibit the accurate prediction of the frequency-response function for thermal shear-stress sensors.[34] Therefore, a direct in situ dynamic calibration is required to determine the transfer function of the sensor. Recently, Sheplak et al.[35] and Chandrasekaran[36] developed a novel, in situ dynamic calibration technique for shear-stress sensors. This technique provides known sinusoidal shear-stress perturbations generated via acoustic plane-wave excitation.

Recently, Breuer et al.,[19] Breuer,[20] and Cain et al.[21] presented similar device designs that achieved thermal isolation using a vacuum cavity obtained via a wafer-bond, thin-back process. The thermal sensor used in this study consists of a 1500 Å $\times$ 4 μm $\times$ 200 μm platinum element on top of a 1500-Å-thick silicon-nitride membrane, which seals a 200-μm-diam and 10-μm-deep vacuum cavity.[21] The advantages of platinum-based sensors over polycrystalline silicon-based sensors include higher TCR, higher thermal operating range, lower impedance, reduced $1/f$ noise, and no piezoresistive-induced pressure sensitivity.[21] Figure 1 is a cross-sectional schematic of the sensor showing the membrane stretched over the vacuum cavity. Two gold leads at each end of the sensing element permit four-point probe characterization to isolate the sensor performance from the effects of the biasing and compensation circuitry. The details of the sensor design and fabrication process flow have been described previously.[19,21,37] The characterization of this device is discussed in the following sections.

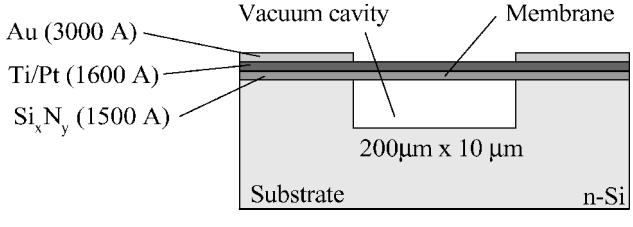

Fig. 1 Cross-sectional schematic of the thermal shear-stress sensor.

Experimental Setup

The experiments were performed in the Interdisciplinary Microsystems Laboratory at the University of Florida. The characterization of the shear-stress sensor included resistance–temperature measurements, static calibrations, and dynamic sensitivity experiments. Noise floor and pressure sensitivity experiments are also described.

Resistance–Temperature Setup

The resistance–temperature behavior, specifically the TCR, of the thin-film platinum sensor is necessary to calculate the sensor overheat ratio for a given resistance. Whereas the TCR of bulk platinum is well documented, its thin-film equivalent may be vastly different.[38] Because this value varies with the thickness and deposition conditions, it must be experimentally determined. A high-temperature measurement apparatus, similar to the one described by Firebaugh,[39] was constructed to permit a four-point probe resistance measurement within a controlled variable thermal environment.[37] For all experiments described here, the sensors were operated in an uncompensated CC mode.

Static Calibration Setup

Static calibration of the sensor was performed in two different environments. An 8.5 mm $\times$ 8.5 mm $\times$ 101.5 cm long duct, that is, a plane-wave tube, provided a maximum mean shear stress of 0.08 Pa and the ability for dynamic-response characterization, as will be described. A 100 $\times$ 1 mm laminar flow channel provided a higher maximum shear stress of 1.7 Pa. The sensor was calibrated in a fully developed incompressible laminar flow in both cases. Incompressible flow was verified by monitoring the pressure drop in the channel. Details of the two setups can be found in Refs. 36 and 37.

Dynamic Calibration Setup

The dynamic calibration technique, based on Stokes layer excitation, utilizes acoustic plane waves to generate a known oscillatory wall shear stress.[35,36] The basic principle of this technique relies on the fact that the particle velocity of the acoustic waves must equal zero at the wall due to the no-slip boundary condition. This leads to the generation of a frequency-dependent boundary layer and wall shear stress.

The dynamic calibration was carried out in a plane-wave tube (PWT) capable of supporting variable mean flows.[36] The low-frequency cutoff for the PWT is 20 kHz. Compliant tubing was used at the duct exit to minimize acoustic reflections.

A microphone (B&K 4138) is mounted at the same axial location as the thermal shear-stress sensor to compute the shear stress generated by the acoustic wave. A Stanford Research Systems SR785 spectrum analyzer serves as the signal source and the data acquisition unit. The speakers are driven by the source signal amplified by a Techron 7540 two-channel amplifier. It can be shown that the theoretical fluctuating shear stress τ' is proportional to the amplitude of the pressure perturbation p' and the square root of excitation frequency[33]:

$$\tau'(\omega, t) = (-p'/c)e^{j\omega t}\sqrt{(j\omega\mu/\rho)}\left[\tanh\left(a\sqrt{j\omega/\upsilon}\right)\right] \qquad (4)$$

where c is the isentropic speed of sound and ω is the angular frequency. For a sinusoidal shear perturbation much less than the established mean, that is, $\tau' \ll \bar{\tau}$, the normalized frequency-response function (FRF), $H(\omega)$ is given by[35]

$$H(\omega) = \frac{V(\omega)/\tau'(\omega)}{\partial\bar{V}/\partial\bar{\tau}} \qquad (5)$$

where $V(\omega)$ is the fluctuating output voltage of the sensor and $\partial\bar{V}/\partial\bar{\tau}$ is the static sensitivity.

Results and Discussion

Temperature–Resistance Results

The nominal unheated resistance of the sensor was on the order of 90 Ω. Thermal–electric measurements indicated a TCR of $0.0029^\circ C^{-1}$ possessing a maximum nonlinearity of 2.7% over a temperature range of 20–400°C (Fig. 2). This represents a reduction

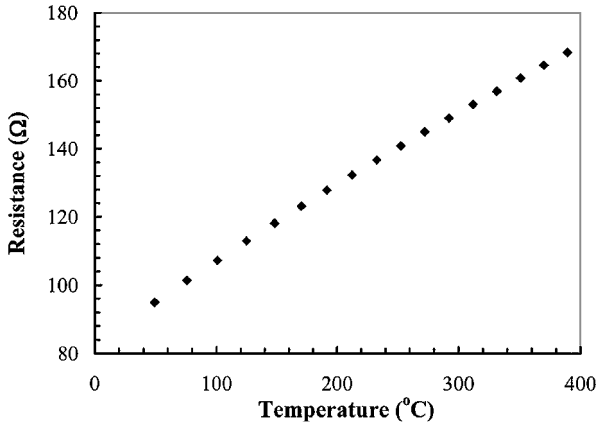

Fig. 2 Resistance vs temperature relationship for the thin-film platinum-sensing element.

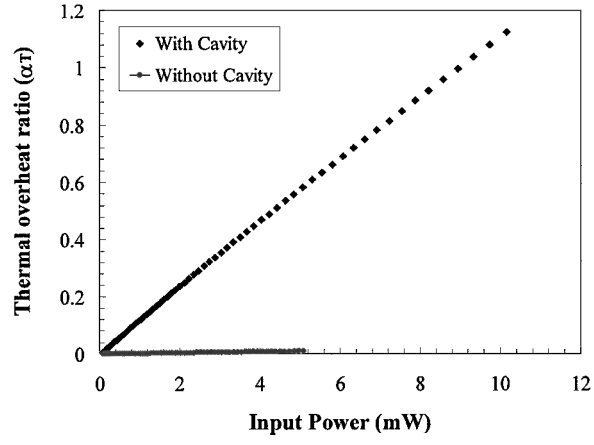

Fig. 3 Thermal overheat ratio vs input power for sensors with and without cavities.

in sensor resistance and an improvement in TCR over polysilicon-based thermal sensors (2 kΩ and 0.0013°C^{-1}, respectively).[13]

The thermal isolation effectiveness of the vacuum cavity is shown in Fig. 3, which shows the sensor overheat as a function of input power for sensors fabricated with and without a cavity. The sensors possessing cavities exhibited much greater overheat than those without cavities. The sensors without cavities could only achieve a maximum overheat of 0.01 before exceeding a destructive current density limit of 1×10^7 A/cm^2. As shown in Fig. 3, the present sensor achieves an overheat ratio of ~0.7 with 6-mW input power. This represents a 50% reduction in power consumption vs similarly sized polysilicon-based sensors at identical operating conditions.[13]

Static Calibration

Static sensitivity experiments were performed in the CC mode of excitation for thermal overheats of 0.2–1.0 and wall shear stresses from 0 to 1.7 Pa. Figures 4 and 5 show the nonlinear static response of the sensor for varying mean shear stress with respect to zero flow condition for the laminar flow channel and PWT, respectively. In both cases, the sensor output voltage increases with overheat ratio α_T. When it is assumed that a hot-film sensor behaves in a manner similar to that of a hot wire, then operating at high α_T has the advantage that the sensor is much more sensitive to shear-stress fluctuations than flow temperature fluctuations.[40] In Fig. 5, an overlap between α_T of 0.9 and 1.0 is observed. The likely reason for this overlap is that the convective heat transfer from the sensor to the flow may be a combination of buoyant and forced convection.

A plot of the static sensitivity $\partial \bar{V} / \partial \bar{\tau}$ at varying mean shear stress is given in Fig. 6 for the laminar flow channel. The static sensitivity decreases with increasing mean shear stress for a fixed overheat ratio at the same time that the sensitivity increases with increasing α_T. This behavior is similar to that of a hot wire.[40]

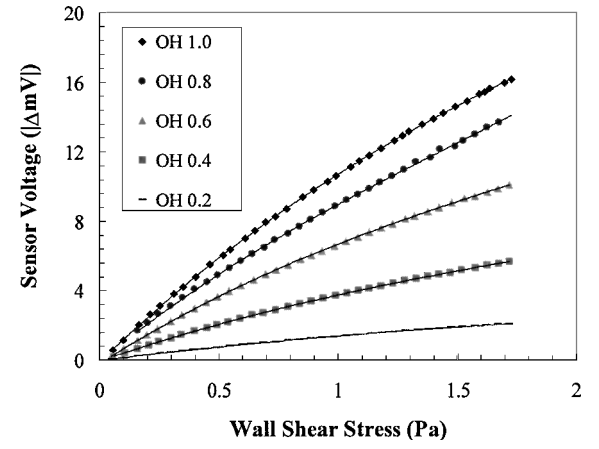

Fig. 4 Static response of the sensor vs shear stress at different overheat ratios, calibrated in the laminar flow channel (third-order polynomial curve fits included).

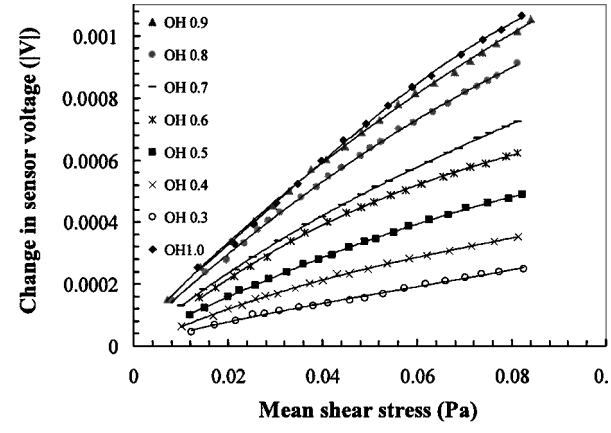

Fig. 5 Static response of the sensor vs shear stress at different overheat ratios, calibrated in the PWT (third-order polynomial curve fits included).

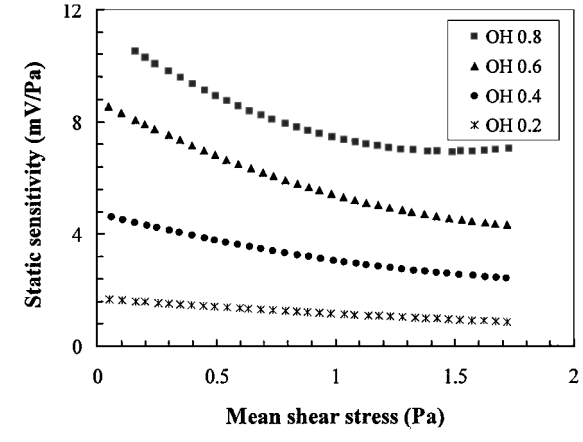

Fig. 6 Static sensitivity of the sensor vs mean shear stress in laminar flow channel.

Note that the static sensitivity data reported here are for the uncompensated sensor. As a result, these data cannot be directly compared with static sensitivity data of compensated sensor systems.

Dynamic Calibration

The sensor was dynamically calibrated using a constant amplitude acoustic tone [105-dB sound pressure level (SPL) with regard to 20 μPa] at multiple overheat ratios (0.6–1.0) and mean shear-stress levels (0.03–0.05 Pa). The SPL of 105 dB and the frequency range of 0.2–7 kHz represent a theoretical fluctuating shear-stress envelope of approximately 0.9 mPa at 200 Hz to 6.1 mPa at 7 kHz. The gain

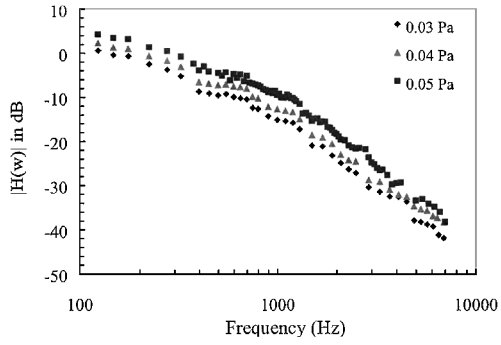

Fig. 7 Gain factor of the sensor frequency response for a 105-dB SPL sine sweep as a function of mean shear stress.

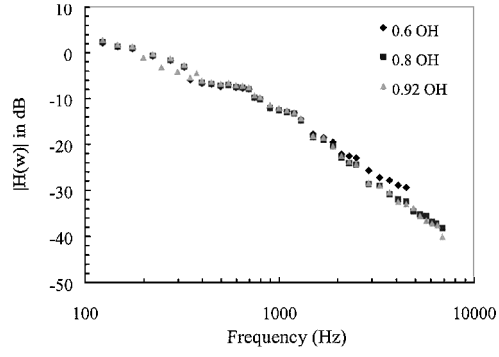

Fig. 8 Plot of the gain factor of the sensor frequency response for a 105-dB SPL sine sweep as a function of overheat ratios.

factor of the FRF, given by Eq. (4), is shown in Fig. 7 for different mean shear stress levels and in Fig. 8 for different overheat ratios. The uncompensated sensor response lies above the noise floor up to 7 kHz, with the −3-dB point at approximately 600 Hz. The dynamic response apparently increases with mean shear stress. This increased dynamic sensitivity is in contrast to the decreased static sensitivity at higher values of mean shear stress, as shown in Fig. 6. This behavior also is similar to that of a hot wire.[40] However, note the possibility that this variation could also be due to mean temperature variations. This issue warrants further study.

Ideally, the gain factor of the FRF would be 0 dB for all frequencies, corresponding to equal static and dynamic sensitivities. However, as already mentioned, the thermal inertia of the uncompensated sensor will cause a rolloff in the FRF with increasing frequency. In both Figs. 7 and 8, the monotonic rolloff in the gain factor is approximately 40 dB/decade and is devoid of a resonance peak, which is indicative of a highly damped second-order system.

Previously, a one-half-order system was used to model the response of a shear-stress sensor on a semi-infinite substrate.[41] The difference in the response of this sensor may be explained by the presence of a 10-μm-deep vacuum cavity that reduces the unsteady heat conduction into the substrate. For this sensor, heat conduction effects are confined to the thin silicon-nitride membrane (see Fig. 3).

To verify the linear relationship between the output voltage fluctuations and the shear stress perturbation, the sensor was excited using acoustic waves of varying amplitude (90–120-dB SPL) at constant frequencies. Figure 9 confirms this linear relationship.

The phase difference between the input pressure signal and the sensor output voltage fluctuation was also estimated using the cross spectrum and is shown in Fig. 10. Theoretically, the shear stress leads the pressure signal by 45 deg (Ref. 42). This is consistent with the interpretation that the voltage fluctuations of the sensor are in phase with the shear-stress perturbations at low frequencies. The dynamic calibration was limited to frequencies greater than 200 Hz. From Fig. 10, it does not appear that the phase has reached an asymptotic limit of 0 deg at ~200 Hz. Further research is required to ascertain the low-frequency behavior of the sensor.

For very large frequencies, the sensor exhibits a 180-deg phase shift characteristic of a second-order-system. However, at ~600 Hz

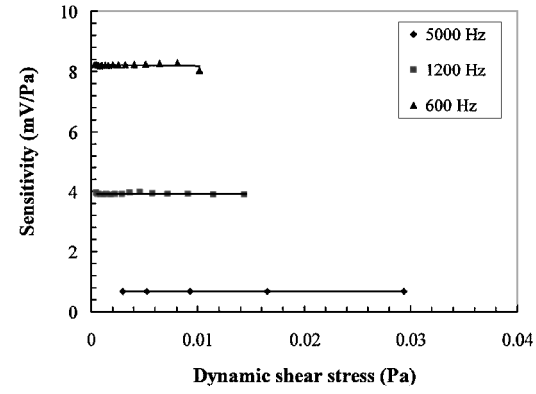

Fig. 9 Linear behavior of the sensor vs the fluctuating shear stress for a constant overheat ratio of 0.81 and a mean shear stress of 0.03 Pa.

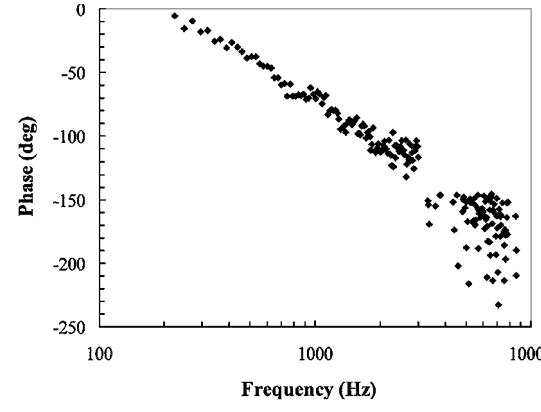

Fig. 10 Phase difference with respect to applied shear stress of the sensor FRF in response to a 105-dB SPL sine sweep.

(the −3-dB point), the phase shift is roughly 45 deg, which is indicative of a first-order system. Thus, the sensor appears to transition from a first-order to a second-order system with increasing frequency. Note that measurements obtained beyond 4 kHz display considerable scatter. This is because both the coherence functions (not shown) approach zero because the signal approaches the noise floor, even after significant averaging.

The transition from a first-order to a second-order system may be physically described in terms of two time constants. The phenomenon of two distinct time constants has been discussed by Haritonidis.[1] At low frequencies, the response of the sensor will be dictated primarily by the substrate. At higher frequencies, the response will likely be a function of the film size and its electrical leads. If the two time constants associated with the diaphragm and the film are close to each other, it may give rise to the transitional behavior observed in the FRF. Clearly, this phenomenon warrants further investigation.

Pressure Sensitivity and Noise Measurements

Two additional metrics of sensor performance are the sensitivity to nonshear-stress inputs and the device noise floor. Experiments were performed to quantify both the pressure sensitivity and the noise floor. The dynamic pressure sensitivity spectrum was determined via a PWT by orienting the sensor at normal incidence to the acoustic waves under zero mean flow conditions. Frequency sweeps at multiple SPL ranging from 120 to 155 dB at a constant overheat ratio of 1.0 were used for the measurements. The results indicate negligible pressure sensitivity (<1 μV/Pa) up to 10 kHz.

The noise floor spectra at zero mean flow and multiple overheat ratios were also measured and are shown in Fig. 11. Electromagnetic interference appears to be the major contributor at low frequencies with all harmonics decaying by 1 kHz. The noise floor data (<100 nV/$\sqrt{\text{Hz}}$) combined with a nominal static sensitivity of 11 mV/Pa results in a minimum detectable shear stress of 9 μPa/Hz or a dynamic range in excess of 100 dB.

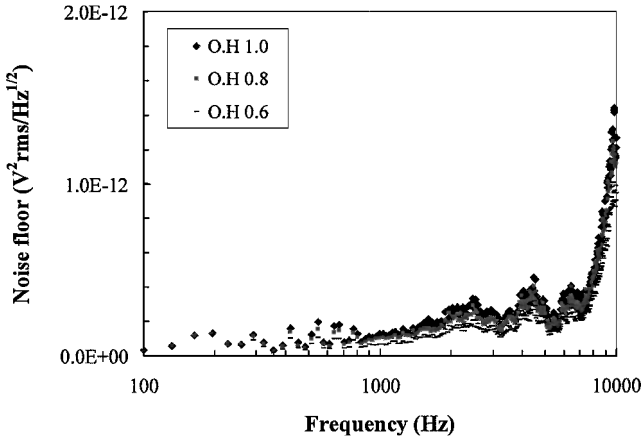

Fig. 11 Measured noise spectrum of the sensor at zero mean shear stress and multiple overheats.

Conclusions

An extensive characterization of an uncompensated, platinum-film, vacuum-cavity silicon-micromachined thermal shear-stress sensor was performed. The sensor was operated in a constant current mode and characterized using a four-point probe configuration to isolate the sensor response from the effects of external compensation circuitry. Noise floor measurements in the operational range of the sensor were obtained and indicate a minimum detectable shear stress of 9 μPa/Hz. Therefore, the dynamic range of the uncompensated sensor exceeds five orders of magnitude (9 μPa–1.7 Pa). The static sensitivity increases with increasing overheat ratio and decreases with increasing mean shear stress. The sensitivity to pressure and its effect on the dynamic response was measured and is negligible.

The sensor was also dynamically calibrated via a known, direct sinusoidal shear-stress input over a frequency range of 0.2–7 kHz. The uncompensated sensor displays characteristics of a two time-constant system with an initial corner frequency of ~600 Hz and a 40 dB/decade rolloff at high frequencies. This behavior differs greatly from the classical one-half-order hot-film response. The measurement and understanding of this uncompensated dynamic behavior is crucial for future sensor optimization and the design of an appropriate feedback compensation circuit to extend the measurement bandwidth.

Other important unresolved issues were also identified. Most of these are concerned with details of the dynamic response characteristics of the sensor. One issue is the inherent temperature sensitivity that can manifest itself as apparent variations in dynamic sensitivity at low frequencies. Clearly, the sensor is sensitive to ambient temperature variations, and a critical study of the suitability of potential temperature correction strategies is warranted. In addition, the flow disturbance due to the heat transfer from the sensor to the flow as a function of overheat ratio needs to be quantified. Furthermore, the dynamic characterization requires clarification in terms of phase response of the sensor at low frequencies. Imperfect termination of the PWT can result in reflected waves, which can affect the response of the sensor. Such reflections should be accounted for in the data reduction process. Finally, a two time-constant hypothesis was postulated as a possible physical explanation of the apparent transition of the uncompensated sensor response from a first-order to a second-order system with increasing frequency. Further experimental, theoretical, and computational studies are required to validate this hypothesis.

Acknowledgments

Partial support for this work was provided by Air Force Office of Scientific Research Contract F4962-97-1-0507. The thermal shear-stress sensors characterized in this paper were designed and fabricated at the Microsystems Technology Laboratory at the Massachusetts Institute of Technology (MIT). The authors thank Joel Voldman from MIT for his assistance in the sensor fabrication.

References

[1]Haritonidis, J. H., "The Measurement of Wall Shear Stress," *Advances in Fluid Mechanics Measurements*, Springer-Verlag, Berlin, 1989, pp. 229–261.

[2]Breuer, K. S., "Active Control of Wall Pressure Fluctuations in a Turbulent Boundary Layer," FED Vol. 168, American Society of Mechanical Engineers, Fairfield, NJ, 1993, pp. 39–48.

[3]Schmidt, M. A., Howe, R. T., Senturia, S. D., and Haritonidis, J. H., "Design and Calibration of a Microfabricated Floating-Element Shear-Stress Sensor," *Transactions of Electron Devices*, Vol. ED-35, 1988, pp. 750–757.

[4]Ng, K., Shajii, J., and Schmidt, M. A., "A Liquid Shear-Stress Sensor Using Wafer-Bonding Technology," *Journal of Microelectromechanical Systems*, Vol. 1, No. 2, 1992, pp. 89–94.

[5]Goldberg, H. D., Breuer, K. S., and Schmidt, M. A., "A Silicon Wafer-Bonding Technology for Microfabricated Shear-Stress Sensors with Backside Contacts," *Proceedings of Solid-State Sensor Actuator Workshop*, Hilton Head, SC, 1994, pp. 111–115.

[6]Padmanabhan, A., Goldberg, H. D., Schmidt, M. A., and Breuer, K. S., "A Wafer-Bonded Floating-Element Shear-Stress Microsensor with Optical Position Sensing by Photodiodes," *Journal of Microelectromechanical Systems*, Vol. 5, No. 4, 1996, pp. 307–315.

[7]Padmanabhan, A., Goldberg, H. D., Schmidt, M. A., and Breuer, K. S., "A Silicon Micromachined Sensor for Shear Stress Measurements in Aerodynamic Flows," AIAA Paper 96-0422, Jan. 1996.

[8]Padmanabhan, A., "Silicon Micromachined Sensors and Sensor Arrays for Shear Stress Measurements in Aerodynamic Flows," Ph.D. Dissertation, Dept. of Mechanical Engineering, Massachusetts Inst. of Technology, Cambridge, MA, Jan. 1997.

[9]Padmanabhan, A., Sheplak, M., Breuer, K. S., and Schmidt, M. A., "Micromachined Sensors for Static and Dynamic Shear Stress Measurements in Aerodynamic Flows," *Transducers '97*, Chicago, 1997, pp. 137–140.

[10]Pan, T., Hyman, D., Mehregany, M., Reshotko, E., and Garverick, S., "Microfabricated Shear Stress Sensors, Part 1: Design and Fabrication," *AIAA Journal*, Vol. 37, No. 1, 1999, pp. 66–72.

[11]Hyman, D., Pan, T., Reshotko, E., and Mehregany, M., "Microfabricated Shear Stress Sensors, Part 2: Testing and Calibration," *AIAA Journal*, Vol. 37, No. 1, 1999, pp. 73–78.

[12]Oudheusden, B., and Huijsing, J., "Integrated Flow Friction Sensor," *Sensors and Actuators A*, Vol. 15, No. 2, 1988, pp. 135–144.

[13]Liu, C., Tai, Y. C., Huang, J., and Ho, C. M., "Surface Micromachined Thermal Shear Stress Sensor," *Proceedings of ASME Symposium on Application of Microfabrication to Fluid Mechanics*, American Society of Mechanical Engineers, Fairfield, NJ, 1994, pp. 9–15.

[14]Jiang, F., Tai, Y. C., Gupta, B., Goodman, R., Tung, S., Huang, J. B., and Ho, C. M., "A Surface-Micromachined Shear Stress Imager," *Proceedings, 1996 IEEE Micro Electro Mechanical Systems Workshop (MEMS '96)*, San Diego, CA, 1996, pp. 110–115.

[15]Liu, C., Huang, C.-B., Zhu, Z., Jiang, F., Tung, S., Tai, Y.-C., and Ho, C.-M., "A Micromachined Flow Shear-Stress Sensor Based on Thermal Transfer Principles," *Journal of Microelectromechanical Systems*, Vol. 8, No. 1, 1999, pp. 90–99.

[16]Kälvesten, E., "Pressure and Wall Shear Stress Sensors for Turbulence Measurements," Ph.D. Dissertation, Dept. of Signals, Sensors and Systems, Royal Inst. of Technology, Stockholm, April 1996.

[17]Kälvesten, E., Stemme, G., Vieider, C., and Löfdahl, L., "An Integrated Pressure-Flow Sensor for Correlation Measurements in Turbulent Gas Flows," *Sensors and Actuators A: Physical*, Vol. 52, No. 1–3, 1996, pp. 51–58.

[18]Lofdahl, L., Kalvesten, E., Hadzianagnostakis, T., and Stemme, G., "An Integrated Silicon Based Wall Pressure-Shear Stress Sensor for Measurements in Turbulent Flows," *ASME Microelectromechanical Systems Subdivision 1996*, American Society of Mechanical Engineers, Fairfield, NJ, 1996, pp. 245–251.

[19]Breuer, K. S., Bayt, R. L., and Nayaar, A., "Measurement of Shear Stress and Temperature Using MEMS Fabricated Sensors," *ASME Microelectromechanical Systems Subdivision 1999*, Vol. 1, American Society of Mechanical Engineers, Fairfield, NJ, 1999, pp. 229–233.

[20]Breuer, K. S., "MEMS Sensors for Aerodynamic Applications: The Good, the Bad (and the Ugly)," AIAA Paper 2000-0251, 2000.

[21]Cain, A., Chandrasekaran, V., Nishida, T., and Sheplak, M., "Development of a Wafer-Bonded, Silicon Nitride Membrane Thermal Shear-Stress Sensor with Platinum Sensing Element," *Proceedings of Solid-State Sensor Actuator Workshop*, Hilton Head, SC, 2000, pp. 300–303.

[22]Löfdahl, L., and Gad-el-Hak, M., "MEMS-Based Pressure and Shear Stress Sensors for Turbulent Flows," *Measurement Science and Technology*, Vol. 10, No. 8, 1999, pp. 665–686.

[23]Naughton, J. W., and Sheplak, M., "Modern Skin-Friction Measurement Techniques: Description, Use, and What to do With the Data," AIAA Paper 2000-2521, 2000.

[24]Bellhouse, B. J., and Schultz, D. L., "The Measurement of Fluctuating Skin Friction in Air with Heated Thin-Film Gauges," *Journal of Fluid Mechanics*, Vol. 32, Pt. 4, 1968, pp. 675–680.

[25]Bellhouse, B. J., and Schultz, D. L., "The Determination of Fluctuating Velocity in Air with Thin Film Gauges," *Journal of Fluid Mechanics*, Vol. 29, No. 2, 1967, pp. 289–295.

[26]Fingerson, L. M., and Freymuth, P., "Thermal Anemometers," *Fluid Mechanics Measurements*, edited by R. J. Goldstein, Hemisphere, New York, 1983, pp. 99–154.

[27]Ludwieg, H., "Instrument for Measuring the Wall Shearing Stress of Turbulent Boundary Layers," NACA TM 1284, 1950.

[28]Ling, S. C., "Heat Transfer from a Small Isothermal Spanwise Strip on an Insulated Boundary," *Journal of Heat Transfer*, Vol. C85, 1963, pp. 230–236.

[29]Ackerberg, R. C., Patel, R. D., and Gupta, S. K., "The Heat/Mass Transfer to a Finite Strip at Small Péclet Numbers," *Journal of Fluid Mechanics*, Vol. 86, 1978, pp. 49–65.

[30]Lin, Q., Jiang, F., Wang, X.-Q., Han, Z., Tai, Y.-C., Lew, J., and Ho, C.-M., "MEMS Thermal Shear-Stress Sensors: Experiments, Theory and Modeling," *Proceedings of Solid-State Sensor Actuator Workshop*, Hilton Head, SC, 2000, pp. 304–307.

[31]Bellhouse, B. J., and Schultz, D. L., "Determination of Mean and Dynamic Skin Friction Separation and Transition in a Low-Speed Flow with a Thin-Film Heated Element," *Journal of Fluid Mechanics*, Vol. 24, 1966, pp. 379–400.

[32]Perry, A. E., Smits, A. J., and Chong, M. S., "The Effects of Certain Low Frequency Phenomena on the Calibration of Hot Wires," *Journal of Fluid Mechanics*, Vol. 90, 1979, pp. 415–431.

[33]Breuer, K. S., "Stochastic Calibration of Sensors in Turbulent Flow Fields," *Experiments in Fluids*, Vol. 19, No. 2, 1995, pp. 133–135.

[34]Brison, J. F., Charnay, G., and Comte-Bellot, G., "Calculation of the Heat Transfer Between a Hot Film and a Substrate Using a Two-Dimensional Model: Prediction of the Dynamic Response for Ordinary Probes," *International Journal of Heat and Mass Transfer*, Vol. 22, No. 1, 1979, pp. 111–119.

[35]Sheplak, M., Padmanabhan, A., Schmidt, M. A., and Breuer, K. S., "Dynamic Calibration of a Shear Stress Sensor Using Stokes Layer Excitation," *AIAA Journal*, Vol. 39, No. 5, 2001, pp. 819–823.

[36]Chandrasekaran, V., Cain, A., Nishida, T., and Sheplak, M., "Dynamic Calibration Technique for Thermal Shear Stress Sensors with Variable Mean Flow," AIAA Paper 2000-0508, 2000.

[37]Cain, A., "Static Characterization of a Micromachined Thermal Shear Stress Sensor," M.S. Thesis, Dept. of Electrical and Computer Engineering, Univ. of Florida, Gainesville, FL, Dec. 1999.

[38]Ohring, M., *The Materials Science of Thin Films*, Academic Press, San Diego, CA, 1992.

[39]Firebaugh, S. L., "Investigation of Materials for Use in High-Temperature, Thin-Film Heaters and Temperature Sensors," M.S. Thesis, Dept. of Electrical Engineering and Computer Science, Massachusetts Inst. of Technology, Cambridge, MA, June 1997.

[40]Perry, A. E., *Hot-Wire Anemometry*, Clarendon, Oxford, 1982, Chaps. 3–4.

[41]Ling, S. C., and Hubbard, P. G., "The Hot Film Anemometer: A New Device for Fluid Mechanics Research," *Journal of the Aerospace Sciences*, Vol. 23, 1956, pp. 890, 891.

[42]White, F. M., *Viscous Fluid Flow*, McGraw–Hill, New York, 1991, pp. 135–141.

W. R. Lempert
Guest Associate Editor